Defect-Dominated Doping and Contact Resistance in MoS_2

Stephen McDonnell,* Rafik Addou, Creighton Buie, Robert M. Wallace, and Christopher L. Hinkle*

Department of Materials Science and Engineering, University of Texas at Dallas, Richardson, Texas 75080, United States

ABSTRACT Achieving low resistance contacts is vital for the realization of nanoelectronic devices based on transition metal dichalcogenides. We find that intrinsic defects in MoS_2 dominate the metal/MoS_2 contact resistance and provide a low Schottky barrier independent of metal contact work function. Furthermore, we show that MoS_2 can exhibit both n-type and p-type conduction at different points on a same sample. We identify these regions independently by complementary characterization techniques and show how the Fermi level can shift by 1 eV over tens of nanometers in spatial resolution. We find that these variations in doping are defect-chemistry-related and are independent of contact metal. This raises questions on previous reports of metal-induced doping of MoS_2 since the same metal in contact with MoS_2 can exhibit both n- and p-type behavior. These results may provide a potential route for achieving low electron and hole Schottky barrier contacts with a single metal deposition.

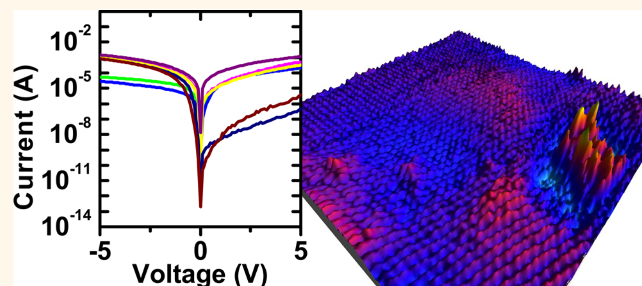

KEYWORDS: defects · MoS_2 · TMD · contacts · Schottky barriers · doping · nanoelectronics

Since the successful demonstration that layered materials including graphite, BN, and MoS_2 could be exfoliated in monolayers,[1] there has been considerable research on the synthesis[2−6] and the integration[7,8] of such materials into nanoelectronic devices. Unlike graphene, the transition metal dichalcogenides (TMDs) can exhibit metallic or semiconducting properties through the proper selection of metal or chalcogen in the crystal, and their band gaps are tunable with thickness, making them suitable for a wide range of electronic and optoelectronic device applications.[9] An early demonstration of a monolayer MoS_2-based field-effect transistor with high (10^8) on/off ratios ignited considerable interest in this material and reported that Au contacts on n-type MoS_2 were ohmic.[10] The reported anomalously low Schottky barrier height for high work function metals, such as Au (Φ_{Au} = 5.1 eV),[11] on n-type MoS_2 has not yet been explained.[10,12−14] In particular, it was shown in a previous study[12] that for MoS_2 devices fabricated with different contact metals (Sc, Ti, Ni, Pt) with work functions ranging from 3.5 to 5.9 eV all exhibited similarly low electron Schottky barrier heights. Understanding the interfaces formed between metals and two-dimensional (2D) semiconductors is critical for controlling contact resistance, which is a limiting factor in device performance and prevents the accurate extraction of the mobilities for these materials.[15−18] The majority of recent studies report n-type behavior with low Schottky barriers even for high work function metals.[14,19−23] Such behavior is not typical of metal/semiconductor contacts without chemical reactions altering the interface. This anomaly has previously been highlighted[12] and attributed to Fermi level pinning close to the conduction band of the MoS_2, but the underlying mechanism is still not understood.

The variability of the electronic properties of MoS_2 from sample to sample and across a sample has only been mentioned briefly in other studies. It was reported that variations in contact resistance from sample to sample make the determination of the intrinsic mobility difficult.[24] A similar variation in contact resistance across a single sample was speculated to be due to defects.[25] It has also been suggested that Au/TMD contacts can be explained by assuming a defective interface.[26] Variations in the extracted mobilities for monolayer devices of more than a factor of 2 even for the same contact metals

* Address correspondence to stephenmcd@utdallas.edu, chris.hinkle@utdallas.edu.

Received for review January 3, 2014 and accepted January 31, 2014.

Published online January 31, 2014
10.1021/nn500044q

© 2014 American Chemical Society

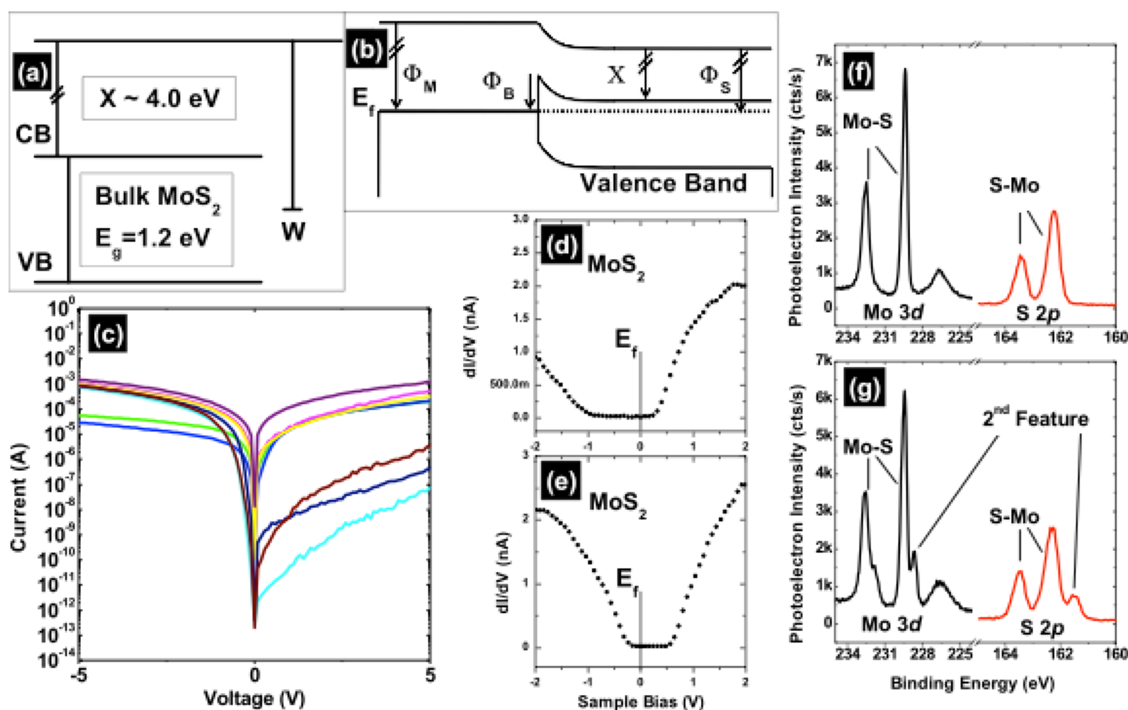

Figure 1. Variability in MoS_2. (a) Schematic of the MoS_2 conduction and valence band levels and the tungsten work function with respect to the vacuum level. (b) Band bending that occurs at a metal semiconductor junction. (c) *I*–*V* characteristics measured on a single piece of MoS_2 with the tungsten probe directly contacting the MoS_2. (d) d*I*/d*V* measured by STS showing the Fermi level near the conduction band for MoS_2. (e) d*I*/d*V* measured by STS showing the Fermi level near the valence band for MoS_2. (f,g) XPS spectra for the Mo 3d, S 2s, and S 2p core-levels acquired from two different areas on the MoS_2 sample.

have also been reported.[10] To date, there has been no study directed at identifying the cause of these variations nor the degree to which they can affect the electronic behavior of the MoS_2.

For this study, we use the same MoS_2 (SPI supplies,[27] cleaned by mechanical exfoliation) reported in recent device studies.[10,14,19,21,28−35] We show that surface defects as well as defect-chemistry-related variations in the local stoichiometry of the MoS_2 can be correlated with the resultant Schottky barrier height in metal/MoS_2 contacts and the n- and p-type behavior of the material. These facts have likely clouded previous studies and possibly led to erroneous conclusions. MoS_2 devices are typically reported in recent literature as exhibiting n-type[2,10,12,29,30,36] behavior; however, we find that it can display both n- and p-type behavior, in agreement with much older studies[37] when reports of both n- and p-type behavior were common. We show that the Schottky barriers between metals and the MoS_2 cannot be predicted by simply comparing the metal work function to the MoS_2 electron affinity. To explain this, we utilize current−voltage (*I*−*V*) measurements carried out with a tungsten probe on multilayer MoS_2 (cleaned by mechanical exfoliation as in other reports)[10,14,19,21,28−32] and correlate the observed trends with variations in the core-level spectra obtained by X-ray photoelectron spectroscopy (XPS), the defect concentration determined by scanning tunneling microscopy (STM), and Fermi level position measured by scanning tunneling spectroscopy (STS). Our unique experimental setup, which allowed the analysis positions for each technique to be mapped across a single sample, enabled the precise correlation between all four techniques, and we show that naturally occurring defects dominate the observed electronic behavior of the MoS_2.

RESULTS AND DISCUSSION

Anomalous Schottky Barrier Heights. In metal/semiconductor contacts where there is no chemical reaction between the metal and semiconductor, the electron Schottky barrier (Φ_b) can be predicted through the relationship

$$\Phi_b = \Phi_m - \chi \quad (1)$$

where Φ_m and χ are the bulk metal work function and semiconductor electron affinity, respectively.[38] This is shown schematically in Figure 1a,b for a W/MoS_2 contact. In Figure 1c, we show for a tungsten probe directly contacting the MoS_2 that the *I*−*V* characteristics vary significantly across a single sample. This highlights the dangers in comparing the *I*−*V* characteristics of different metal/MoS_2 contacts when there is such a large degree of variation for even single metal/MoS_2 contacts. Figure 1d,e shows, by scanning tunneling spectroscopy, that the local position of the Fermi level can vary from close to the conduction band to close to the valence band by moving the analysis

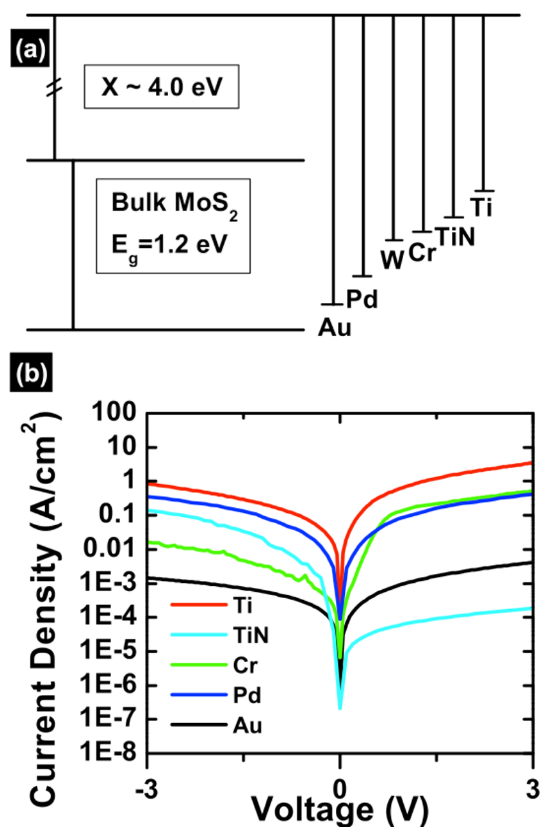

Figure 2. Band alignment and observed $I-V$ characteristics for a range of contact metal work functions. (a) Schematic of the MoS_2 conduction and valence band levels and a range of metal work functions with respect to the vacuum level. (b) Observed $I-V$ characteristics of the metal/MoS_2 contacts.

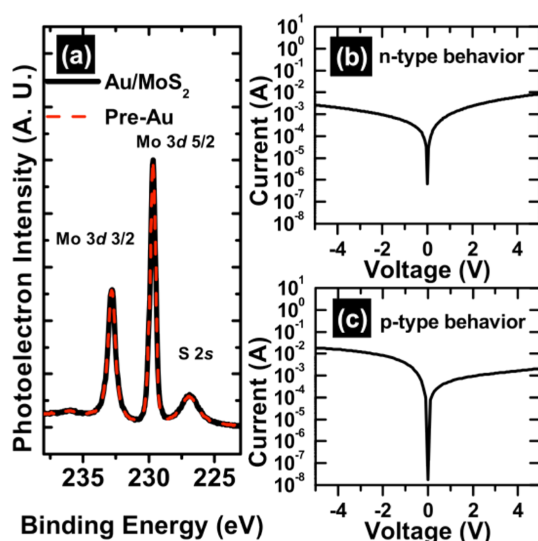

Figure 3. Au contacts with MoS_2. (a) XPS spectra for the Mo 3d and S 2s core-levels acquired before and after Au deposition and aligned to the Mo 3d binding energy position to account for band bending. (b) $I-V$ characteristics from a Au/MoS_2 contact exhibiting "typical" n-type behavior. (c) $I-V$ characteristics from a Au/MoS_2 on the same sample exhibiting p-type behavior.

location on a single MoS_2 sample by even tens of nanometers. Similarly, X-ray photoelectron spectroscopy shows variations in the observed core-level spectra with low binding energy features being detected for the Mo 3d and S 2p core-levels on a large percentage of a sample area.

Any investigations of the metal/MoS_2 interface must differentiate between three effects that will likely cause deviations from eq 1 before any conclusions can be drawn: (i) reactions between the metal and substrate (for example, such as those that occur in Ni/Si contacts where nickel silicide has a lower Schottky barrier than would be expected from the comparison of nickel work function and silicon electron affinity),[11,39] (ii) the inherent variability in the electronic behavior of MoS_2 that was illustrated in Figure 1, and (iii) the reported Fermi level pinning of metals to just below the conduction band of MoS_2.[12]

Metal Reactions with MoS_2. We investigate the electrical and physical properties of metals, with a range of work functions, deposited on MoS_2. Figure 2a shows the theoretical band alignment for Au, Pd, W, Cr, TiN, and Ti.[11] Figure 2b shows the observed $I-V$ characteristics, and it is immediately evident that deposited Ti, Pd, and Au show qualitatively similar characteristics to those observed with the tungsten probe; that is, their reverse bias currents are near the same values as their respective forward bias currents (contrary to what would be expected from their predicted Schottky barrier heights, for Au and Pd in particular).[40] In contrast, Cr and TiN exhibit notably different behavior. Chemical analysis of these interfaces using XPS (shown in the Supporting Information) revealed that both Cr and TiN react with the underlying MoS_2. As such, the resultant contact resistance would be determined by the work function of the metal/MoS_2 alloy contact at the interface, and so these metals will not be considered further for the purpose of this study.

Figure 3a shows an example of the XPS spectra from the Mo 3d and S 2s core-levels before and after Au depositions, and the lack of interfacial reactions can be concluded from the clear overlap of the features. Similar spectra (shown in the Supporting Information) can be obtained for Pd and Ti under controlled deposition conditions. Since there are no detectable chemical reactions between the metals and MoS_2, the Schottky barrier of the contacts should be determined by eq 1. Instead, all three metals show low electron Schottky barrier heights despite the differences in their respective work functions. While this result requires explanation, it is at least consistent with other reports using Au and Ti/Au contacts.[10,12,13] We also find that for Au contacts deposited on a single piece of MoS_2, both n- and p-type characteristics can be observed at different positions. This is shown in Figure 3b,c, where $I-V$ curves obtained from two different contacts on the same piece of MoS_2 display n- and p-type behavior, respectively. The correlation between such $I-V$ characteristics and n- or p-type behavior observed by XPS

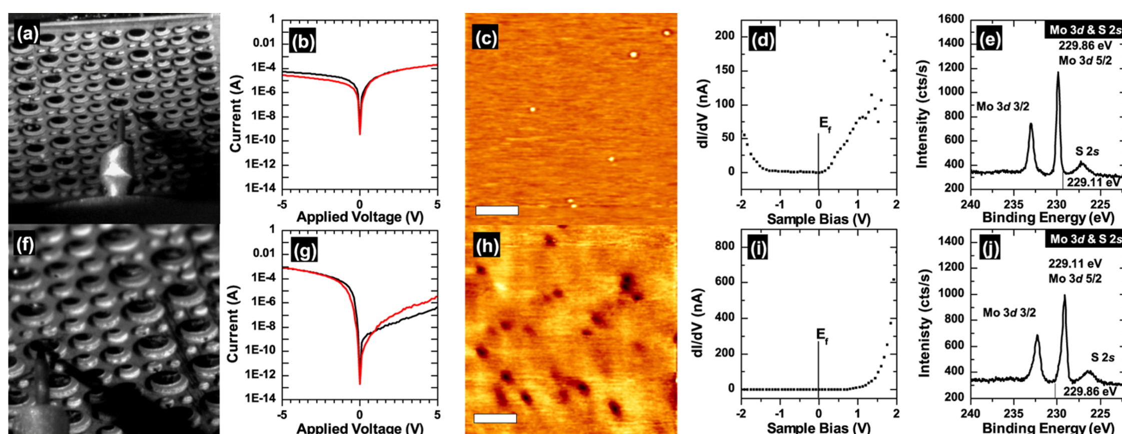

Figure 4. Correlation of $I-V$ characteristics with STM, STS, and XPS. (a) MoS_2 sample covered with a shadow mask to allow positional mapping of the sample. (b) $I-V$ characteristics acquired from within a specific mask aperture showing n-type behavior. (c) STM acquired in the same mask aperture as 4b with both bright and dark defects observed. (d) STS acquired in the same mask aperture as 4b showing the Fermi level close to the conduction band. (e) XPS of the Mo 3d and S 2s core-levels acquired from the same mask aperture as 4b consistent with n-type MoS_2. (f) STM tip scanning in a different shadow mask aperture. (g) $I-V$ characteristics acquired from within a different mask aperture to 4b showing p-type behavior. (h) STM acquired in the same mask aperture as 4g with a comparatively high concentration of dark defects observed. (i) STS acquired in the same mask aperture as 4g showing the Fermi level position more than 1 eV away from the conduction band. (j) XPS of the Mo 3d and S 2s core-levels acquired from the same mask aperture as 4g showing lower binding energy than 4e. STM scale bars are 20 nm, and the scanning conditions are (c) −1.5 V, 0.1 nA, (h) 1.5 V, 1 nA.

and STS will be discussed in the following section. This unexpected finding calls into question claims of apparent p-type doping of MoS_2 using Pd contacts[31] since doping variations are, in fact, observed independent of the contact metal.

Variability in the Electronic Properties of MoS_2. To examine the variability in the electronic behavior across a given sample and correlate electrical, chemical, and structural information, a natural, exfoliated MoS_2 sample was fitted with a shadow mask, which defined regions of interest and thus served as an effective mapping tool. The largest apertures were 500 μm in diameter, which allowed for analysis by XPS, STM, and a tungsten needle probe for $I-V$ measurements all within the same region. Figure 4a,f shows this setup with an approaching STM tip. Regions were selected where the $I-V$ characteristics exhibited either n- (b−e) or p-type (g−j) behavior, and the same regions were analyzed with XPS and STM/STS.

For Figure 4b−e, the $I-V$ characteristics display n-type behavior; the STM shows metallic-like (bright) defects in negative bias at relatively low concentration; the STS shows a Fermi level position close to the conduction band, and the XPS core-level spectra show a single chemical state corresponding to MoS_2. In contrast, Figure 4g−j shows that the $I-V$ characteristics display p-type behavior; the STM shows a high density of structural (dark) defects in positive bias; the STS shows a Fermi level position greater than 1 eV below the conduction band edge, and the XPS core-level spectra are dominated by features shifted 0.8 eV to lower binding energy which is consistent with p-type behavior. To ensure that the observed defects and variations are not simply the result of damage induced by our characterization techniques, we investigated multiple samples and varied the sequence of analysis. For example, when a region with low binding energy features was identified by XPS on a new freshly exfoliated sample, this region would consistently appear highly defective in subsequent STM measurements and also exhibited p-type conduction when the $I-V$ characteristics were measured last. Similarly, a region of p-type conduction identified from the $I-V$ characteristic acquired from a new sample would consistently show low binding energy features in subsequent XPS analysis and appear highly defective when STM was carried out last. Scanning tunneling microscopy carried out on separate, freshly exfoliated samples showed that as received MoS_2 can have localized regions of high or low defect density, with some defects being metallic while the Fermi level position, determined by STS, was found to vary by ∼1 V. These additional observations confirmed that the defects shown in Figure 4 are present on as exfoliated MoS_2 and are not a result of damage induced during characterization.

It is now useful to discuss the chemistry of MoS_2 and the defects observed by STM and explain the variations in the core-level spectra. The stoichiometry of n-type MoS_2 appears to be ∼1.8:1 (S/Mo) as determined by XPS. This would be consistent with the presence of sulfur vacancies that would cause n-type behavior. While the presence of a low binding energy feature in the Mo 3d core-level could easily suggest the detection of metallic Mo, the similar feature detected in the S 2s and S 2p core-levels makes this assignment unlikely since elemental S should appear at a higher binding energy[41] to MoS_2, which can be estimated from electronegativity arguments. Since the binding

energy of core-levels detected in XPS is referenced to the Fermi level of the system, p-type materials will appear at a lower binding energy than n-type materials. As such, the shift of 0.8 eV to lower binding energy can be attributed to a 0.8 eV shift in the Fermi level position closer to the valence band edge and not the existence of a new chemical state. In addition, if the Mo 3d and S 2p spectra are deconvolved into features correlated to n-type (high binding energy) and p-type (low binding energy) related features, we can calculate the stoichiometry for each. We find that for the n-type region the ratio of S/Mo is still ∼1.8:1; however, in the p-type region, the stoichiometry is 2.3:1, indicating that these regions are either sulfur-rich (anti-sites, intercalates, or interstitials) or molybdenum-deficient (molybdenum vacancies).[42] Since sulfur-deficient and sulfur-rich MoS_2 would be expected to result in n-type and p-type behavior, respectively, the changes in stoichiometry, binding energy position, $I-V$ characteristics, and Fermi level position (measured by STS) are all consistent.

As noted previously, there are two distinct types of defects on the as-received MoS_2 observed by STM, and both are very similar to those induced by Ar^+ irradiation of MoS_2, reported recently.[43] One defect appears to be dark in both positive and negative bias, while the other appears dark in positive bias but bright in negative bias (*i.e.*, when probing filled states).[43] This is illustrated in the Supporting Information Figure S2. The bright defects observed in negative bias can be described as metal-like regions of low sulfur concentration (*i.e.*, Mo-like clusters) confirmed to be metallic by STS. Dark pits ∼0.7 nm deep were attributed to missing MoS_2 layers either on or beneath the surface, and STS obtained from the center of such defects was found to be similar to that on defect-free regions but with the Fermi level shifted 0.2 eV away from the conduction band. On the edges of these defects, the band gap appeared to be lowered.

It is interesting that in our work we identify the presence of both types of defects in large concentrations on commercially available[27] MoS_2 that has not been intentionally damaged by Ar^+ irradiation. The significance of metallic-like defects will be discussed further in the following section, but the correlation between the high densities of "dark" defects, p-type behavior, and higher S/Mo ratio is clear. Previous STM reports[43] showed that such dark defects are present in both positive and negative bias, suggesting that the defects are structural. We speculate that these defects are formed to reduce strain in areas of high sulfur concentration. These defects can therefore be viewed as a signature of a high S/Mo ratio and thereby correlate with the observed p-type behavior (from $I-V$, XPS, and STS) and the stoichiometry change detected by XPS.

For the areas of comparatively lower defect concentration, which exhibit n-type $I-V$ characteristics

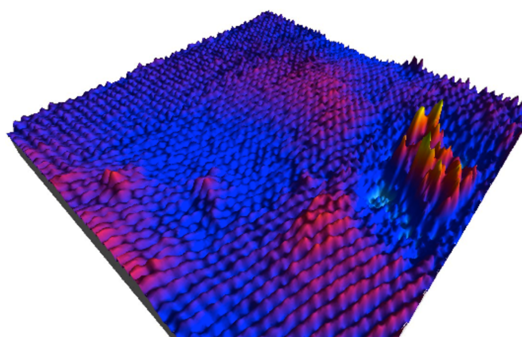

Figure 5. Three-dimensional image showing a high tunneling current from a defect of a 13.6 × 13.6 nm three-dimensional STM image of the MoS_2 surface with atomic resolution acquired in negative bias. This image illustrates the higher conductivity of certain defects on the surface, which are attributed to metallic clusters. The imaging conditions were −100 mV, 0.5 nA.

and core-level binding energies, it is the bright defects that are the most interesting. Such bright defects are visible only in negative bias (shown in the Supporting Information), which means that it is an increase in tunneling current rather than a topographical protrusion that is being observed. Figure 5a shows an atomic resolution image of the MoS_2 surface and illustrates how the tunneling current through these defect regions is higher than that of the surrounding MoS_2. Such an increase in current would be expected from a metallic-like region. Since these defects are detected in any 100 × 100 nm scan, it can therefore be safely assumed that micrometer-sized metal contacts, typically exploited in recent research reports,[10,14,19,21,28−32] will necessarily contact both ideal and defective MoS_2, and therefore, the actual Schottky barrier height will be modified from the simple form of eq 1, even in situations where no metal/MoS_2 reactions have been detected. In fact, these observed metallic-like defects effectively turn these Schottky contacts into inhomogeneous metal/MoS_2 junctions with the majority of the junction area comprising the deposited metal/MoS_2 interface as expected and a small area comprising the metallic-like defect/MoS_2 interface. Using the STM, we can estimate that these defects have an areal density on the order of 0.1−5% in n-type regions, and conduction through these metallic-like defect/MoS_2 contact regions should be independent of the deposited contact metal.

Impact of Defective MoS_2 on the Schottky Barrier Height. For an inhomogeneous interface where a semiconductor is effectively in contact with metals of different work functions, the junction current can be described using a parallel conduction model. If we assume that the bright defects observed by STM/STS behave as metals with a low work function, then this inhomogeneous model (described in the Supporting Information) can describe the observed Schottky diode currents observed in our experiments. Figure 6a shows the observed junction currents for three nonreacting metals on MoS_2.

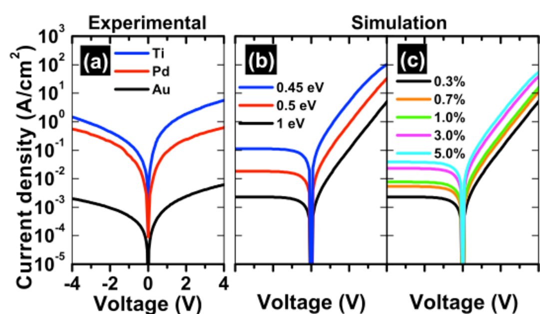

Figure 6. Comparison of the experimental and simulated *I*−*V* characteristics. (a) Experimental *I*−*V* characteristics of Ti/MoS_2, Pd/MoS_2, and Au/MoS_2 for comparison to the simulated curves (b,c). (b) Simulated *I*−*V* characteristics for an inhomogeneous interface assuming fixed defect areal density of 0.3% with metal electron Schottky barriers of 0.45, 0.5, and 1 eV. (c) Fixed metal electron Schottky barrier of 1 eV and varying defect areal density of 0.3, 0.7, 1, 3, and 5%. Both (b) and (c) assume the defect electron Schottky barrier to be 0.4 eV and series resistance of 25 Ω.

Figure 6b shows three calculated junction currents, assuming this inhomogeneous junction and purely thermionic emission, for three different deposited work function metals along with the observed metallic-like defects. For this simple model, the total current is equal to the linear sum of the current through the deposited metal/ideal MoS_2 area and the low work function metal/defect MoS_2 area in an area ratio of 99.7:0.3, consistent with STM imaging.

Assuming a high work function metal with a Schottky barrier height 0.6 eV greater than the defect (with 0.3% coverage), the calculated currents are several orders of magnitude higher than a junction with no defects (shown in the Supporting Information, Figure S3). This is because the junction current is dominated by the current through the defects, owing to the low effective work function in that region and the exponential dependence of the current on the resultant lower Schottky barrier height. Even for such a low areal density of 0.3%, the current is primarily determined by the Schottky barrier of the defects. However, the deposited metal work function still does have an impact on the overall current levels as is seen in Figure 6b. For high work function and the correspondingly high Schottky barrier height metals, such as Au, the overall current levels in both forward and reverse bias are orders of magnitude lower than when the Schottky barrier height of the deposited metal is near that of the defect. The trends shown by these calculations agree well with the experimental data shown in Figure 6a, with the total junction current increasing with decreasing metal work function, but still being primarily influenced by the low Schottky barrier height defects.

Figure 6c shows the impact on the simulated currents for a single metal contact as the areal percentage of defects in the junction is increased. It is clear that while the presence of even low concentrations of defects dominate the observed Schottky barrier and result in apparent Fermi level pinning of the metals, the variations in defect density also strongly impact the measured currents.

Correlating Doping Variations and Defect-Mediated Schottky Barrier Lowering with Other Works. In recent reports, it has generally been accepted that MoS_2 is an n-type semiconductor. While sulfur vacancies are an obvious cause of n-type behavior (vacuum annealing has been reported to dope MoS_2 with n-type carriers[21]), such observations are typically not attributed to sulfur vacancies due to previous work[44] which demonstrated the thermal stability of MoS_2 under vacuum annealing, showing no weight loss until 930 °C and no desorbed sulfur detected until 1090 °C. Another study[28] chose instead to attribute this behavior to low concentrations of Cl and Br impurities detected in natural MoS_2 (obtained from SPI supplies). However, such impurities are not typically reported nor are they detected here. Instead, variations in the ratio of S/Mo are seen to vary across a single sample by up to 30%, which is direct evidence that the stoichiometry in natural MoS_2 is not uniform. This is consistent with the atomic level defects, many of which show a metallic nature and have previously been attributed to areas of low sulfur concentration.[43] As such, it can be concluded that the sulfur vacancies are present in high enough concentrations to be detectable by STM without any thermal treatments and should contribute to the n-type behavior of MoS_2.

The p-type behavior observed in early studies[37] and also here can be correlated with areas of higher S/Mo concentration and high defect density. Scanning tunneling spectroscopy measurements taken in these regions show a large degree of local variability with n-type, p-type, and low band gap spectra all being observed. The global effect of these is the observation of p-type behavior with large variations in the current under positive bias using a tungsten probe directly on the MoS_2 surface. More importantly, the STS shows that variations in the electronic behavior can occur over nanometer scales and implies that variations will typically be present in a micrometer scale exfoliated flake and potentially within a single nanometer scale device.

The simple model proposed here to explain the defect-mediated low Schottky barrier contacts for a wide range of metal work functions requires the defect to behave as a low work function metal and is based on thermionic emission only. Other factors that could potentially influence the overall current in a given metal contact include variations in defect concentration, field emission, and metal/semiconductor wave function overlap (predicted for metals on graphene to result in an effective lowering of the metal work function that may also apply to MoS_2).[45−47] However, none of these effects are inconsistent with the defect-dominated Schottky barrier height model proposed

here, and the strong dependence of the junction current on the density of defects that has been shown in Figure 6c is clear. Such variations, however, prevent a quantitative determination of the position of the defect relative to the MoS_2 conduction band. This is because the exact concentration of defects at the metal/MoS_2 interfaces studied here is unknown and also varies from one contact to another due to the variability in defect concentration across an as-exfoliated MoS_2 surface. Using STM to estimate a realistic defect density range, it appears clear that the defect lies in the top third of the MoS_2 band gap, suggesting Fermi level pinning ~0.2–0.4 eV below the conduction band edge, consistent with previous work.[12] Since the metal-like defects have been identified in our work as the cause of the Schottky barrier height lowering, the effect of Mo defects (caused by sulfur vacancies) should be considered. The reported values[11,48] of Mo work function can vary from 4.2 to 4.6 eV, which suggests that Mo-related defects are a likely cause of the anomalously low Schottky barrier height of high work function metals in contact with MoS_2. The combination of a high work function metal and these low work function metallic-like defects explains the high reverse bias currents for both n- and p-type *I*–*V* characteristics in Figure 3b,c since the inhomogeneous interface results in both low hole (Au/MoS_2) and low electron (defect/MoS_2) Schottky barriers. If sufficient control of the defect density could be obtained, perhaps through MoS_2 synthesis or surface treatments, then the deliberate formation of low hole and low electron Schottky barriers with predictable junction currents could be achieved with a single high work function metal deposition.

CONCLUSIONS

This study has focused on MoS_2 due to the large number of recent reports on MoS_2-based devices, which in turn is related to the relative ease with which natural MoS_2 can be acquired. It is, however, reasonable to assume that the observations made here for MoS_2 will extend to other TMDs. While the correlations between *I*–*V*, XPS, STM, and STS require the use of a single sample (highlighting the variability across a single piece of MoS_2), the observance of p-type behavior, low binding energy features in the core-level spectra, bright and dark defects in STM, and Fermi level shifts in STS have been observed by us on multiple samples acquired from SPI supplies[27] and also on molybdenite samples acquired from Ward's Science,[49] suggesting that these defects are intrinsic to natural exfoliated MoS_2. The large degree of variation in the electronic properties of MoS_2 on both the macroscopic and atomic scale illuminates two key points: (1) high-quality TMDs must be synthesized (including potentially the passivation or control of defect concentrations) in order to truly understand the intrinsic electrical properties; and (2) no claims can be made regarding metal-induced doping of TMDs while the available material displays equal variations in doping with and without metal depositions.

MATERIALS AND METHODS

MoS_2 crystals used here were purchased from SPI supplies.[27] The samples were cleaned by mechanical exfoliation immediately prior to any analysis or loading into UHV. XPS was carried out using a monochromated Al Kα source and an Omicron EA125 hemispherical analyzer. The analyzer acceptance angle of 8°, takeoff angle of 45°, and pass energy of 15 eV were employed in this study. Spectra were deconvolved using the curve fitting software AAnalyzer,[50] and the stoichiometry of the MoS_2 was determined using relative sensitivity factors for the Mo 3d and S 2p core-levels of 2.867 and 0.57, respectively. Metal electron beam depositions of Au, Pd, Ti, and Cr were carried out both in UHV in a clustered chamber attached to the XPS analysis chamber, described elsewhere,[51] and also in an *ex situ* high vacuum e-beam reactor. TiN was sputter deposited on the MoS_2. For device characterization, the metal depositions were carried out through a shadow mask resulting in >20 circular 500 μm diameter contacts. This allowed for multiple identical metal contacts to be compared on a single sample (*e.g.*, Figure 4). For comparisons made between different metals (*e.g.*, Figure 2), the depositions were carried out on different samples. Electrical characterization was performed using a Cascade probe station in conjunction with a HP4155A parameter analyzer. Scanning tunneling microscopy and spectroscopy were carried out using an Omicron VT SPM with an etched tungsten tip.

Conflict of Interest: The authors declare no competing financial interest.

Acknowledgment. The authors would like to thank Dr. Cheng Gong and Dr. Luigi Colombo for useful discussions. This work was supported in part by the Southwest Academy on Nanoelectronics sponsored by the Nanoelectronic Research Initiative and also by the Center for Low Energy Systems Technology (LEAST), one of six centers supported by the STARnet phase of the Focus Center Research Program (FCRP), a Semiconductor Research Corporation program sponsored by MARCO and DARPA.

Supporting Information Available: Additional information including XPS evidence of metal reactions with MoS_2, STM showing bright and dark defects as well as "clean" atomically resolved areas, a full description of the inhomogeneous contact model, justification for the use of current rather than current density in *I*–*V* plots, and a discussion of the possible causes for current level variations from sample to sample. This material is available free of charge *via* the Internet at http://pubs.acs.org.

REFERENCES AND NOTES

1. Novoselov, K.; Jiang, D.; Schedin, F.; Booth, T.; Khotkevich, V.; Morozov, S.; Geim, A. Two-Dimensional Atomic Crystals. *Proc. Natl. Acad. Sci. U.S.A.* **2005**, *102*, 10451–10453.
2. Lee, Y. H.; Zhang, X. Q.; Zhang, W. J.; Chang, M. T.; Lin, C. T.; Chang, K. D.; Yu, Y. C.; Wang, J. T. W.; Chang, C. S.; Li, L. J.; *et al.* Synthesis of Large-Area MoS_2 Atomic Layers with Chemical Vapor Deposition. *Adv. Mater.* **2012**, *24*, 2320–2325.
3. Shi, Y. M.; Zhou, W.; Lu, A. Y.; Fang, W. J.; Lee, Y. H.; Hsu, A. L.; Kim, S. M.; Kim, K. K.; Yang, H. Y.; Li, L. J.; *et al.* van der Waals Epitaxy of MoS_2 Layers Using Graphene as Growth Templates. *Nano Lett.* **2012**, *12*, 2784–2791.

4. Thimsen, E.; Baryshev, S. V.; Martinson, A. B. F.; Elam, J. W.; Veryovkin, I. V.; Pellin, M. J. Interfaces and Composition Profiles in Metal-Sulfide Nanolayers Synthesized by Atomic Layer Deposition. *Chem. Mater.* **2013**, *25*, 313–319.
5. Yu, Y.; Li, C.; Liu, Y.; Su, L.; Zhang, Y.; Cao, L. Controlled Scalable Synthesis of Uniform, High-Quality Monolayer and Few-Layer MoS_2 Films. *Sci. Rep.* **2013**, *3*, 1866.
6. Ismach, A.; Chou, H.; Ferrer, D. A.; Wu, Y. P.; McDonnell, S.; Floresca, H. C.; Covacevich, A.; Pope, C.; Piner, R.; Kim, M. J.; *et al.* Toward the Controlled Synthesis of Hexagonal Boron Nitride Films. *ACS Nano* **2012**, *6*, 6378–6385.
7. Liu, H.; Xu, K.; Zhang, X.; Ye, P. D. The Integration of High-K Dielectric on Two-Dimensional Crystals by Atomic Layer Deposition. *Appl. Phys. Lett.* **2012**, *100*, 152115.
8. Colombo, L.; Wallace, R. M.; Ruoff, R. S. Graphene Growth and Device Integration. *Proc. IEEE* **2013**, *101*, 1536–1556.
9. Wang, Q. H.; Kalantar-Zadeh, K.; Kis, A.; Coleman, J. N.; Strano, M. S. Electronics and Optoelectronics of Two-Dimensional Transition Metal Dichalcogenides. *Nat. Nanotechnol.* **2012**, *7*, 699–712.
10. Radisavljevic, B.; Radenovic, A.; Brivio, J.; Giacometti, V.; Kis, A. Single-Layer MoS_2 Transistors. *Nat. Nanotechnol.* **2011**, *6*, 147–150.
11. Michaelson, H. B. The Work Function of the Elements and Its Periodicity. *J. Appl. Phys.* **1977**, *48*, 4729–4733.
12. Das, S.; Chen, H.-Y.; Penumatcha, A. V.; Appenzeller, J. High Performance Multi-layer MoS_2 Transistors with Scandium Contacts. *Nano Lett.* **2012**, *12*, 100–105.
13. Neal, A.; Liu, H.; Gu, J.; Ye, P. In *Metal Contacts to MoS_2: A Two-Dimensional Semiconductor*; 70th Annual Device Research Conference (DRC), 2012; pp 65−66.
14. Liu, H.; Neal, A. T.; Ye, P. D. Channel Length Scaling of MoS_2 Mosfets. *ACS Nano* **2012**, *6*, 8563–8569.
15. Jena, D. Tunneling Transistors Based on Graphene and 2-D Crystals. *Proc. IEEE* **2013**, *7*, 1585–1602.
16. Seabaugh, A. C.; Zhang, Q. Low-Voltage Tunnel Transistors for Beyond CMOS Logic. *Proc. IEEE* **2010**, *98*, 2095–2110.
17. Fuhrer, M. S.; Hone, J. Measurement of Mobility in Dual-Gated MoS_2 Transistors. *Nat. Nanotechnol.* **2013**, *8*, 146–147.
18. Radisavljevic, B.; Kis, A. Measurement of Mobility in Dual-Gated MoS_2 Transistors. *Nat. Nanotechnol.* **2013**, *8*, 147–148.
19. Wang, H.; Yu, L.; Lee, Y.-H.; Shi, Y.; Hsu, A.; Chin, M. L.; Li, L.-J.; Dubey, M.; Kong, J.; Palacios, T. Integrated Circuits Based on Bilayer MoS_2 Transistors. *Nano Lett.* **2012**, *12*, 4674–4680.
20. Qiu, H.; Pan, L.; Yao, Z.; Li, J.; Shi, Y.; Wang, X. Electrical Characterization of Back-Gated Bi-Layer MoS_2 Field-Effect Transistors and the Effect of Ambient on Their Performances. *Appl. Phys. Lett.* **2012**, *100*, 123104.
21. Baugher, B.; Churchill, H. O.; Yang, Y.; Jarillo-Herrero, P. Intrinsic Electronic Transport Properties of High Quality Monolayer and Bilayer MoS_2. *Nano Lett.* **2013**, *13*, 4212–4216.
22. Liu, H.; Si, M.; Najmaei, S.; Neal, A. T.; Du, Y.; Ajayan, P. M.; Lou, J.; Ye, P. D. Statistical Study of Deep Submicron Dual-Gated Field-Effect Transistors on Monolayer Chemical Vapor Deposition Molybdenum Disulfide Films. *Nano Lett.* **2013**, *13*, 2640–2646.
23. Gourmelon, E.; Bernede, J. C.; Pouzet, J.; Marsillac, S. Textured MoS_2 Thin Films Obtained on Tungsten: Electrical Properties of the W/MoS_2 Contact. *J. Appl. Phys.* **2000**, *87*, 1182–1186.
24. Bao, W. Z.; Cai, X. H.; Kim, D.; Sridhara, K.; Fuhrer, M. S. High Mobility Ambipolar MoS_2 Field-Effect Transistors: Substrate and Dielectric Effects. *Appl. Phys. Lett.* **2013**, *102*, 042104.
25. Maurel, C.; Ajustron, F.; Pechou, R.; Seine, G.; Coratger, R. Electrical Behavior of the Au/MoS_2 Interface Studied by Light Emission Induced by Scanning Tunneling Microscopy. *Surf. Sci.* **2006**, *600*, 442–447.
26. Monch, W. Valence-Band Offsets and Schottky Barrier Heights of Layered Semiconductors Explained by Interface-Induced Gap States. *Appl. Phys. Lett.* **1998**, *72*, 1899–1901.
27. SPI Supplies, http://www.2spi.com/.
28. Yin, Z. Y.; Li, H.; Li, H.; Jiang, L.; Shi, Y. M.; Sun, Y. H.; Lu, G.; Zhang, Q.; Chen, X. D.; Zhang, H. Single-Layer MoS_2 Phototransistors. *ACS Nano* **2012**, *6*, 74–80.
29. Li, H.; Yin, Z.; He, Q.; Li, H.; Huang, X.; Lu, G.; Fam, D. W. H.; Tok, A. I. Y.; Zhang, Q.; Zhang, H. Fabrication of Single- and Multilayer MoS_2 Film-Based Field-Effect Transistors for Sensing NO at Room Temperature. *Small* **2012**, *8*, 63–67.
30. Kim, S.; Konar, A.; Hwang, W. S.; Lee, J. H.; Lee, J.; Yang, J.; Jung, C.; Kim, H.; Yoo, J. B.; Choi, J. Y.; *et al.* High-Mobility and Low-Power Thin-Film Transistors Based on Multilayer MoS_2 Crystals. *Nat. Commun.* **2012**, *3*, 1011.
31. Fontana, M.; Deppe, T.; Boyd, A. K.; Rinzan, M.; Liu, A. Y.; Paranjape, M.; Barbara, P. Electron−Hole Transport and Photovoltaic Effect in Gated MoS_2 Schottky Junctions. *Sci. Rep.* **2013**, *3*, 1634.
32. Bertolazzi, S.; Krasnozhon, D.; Kis, A. Nonvolatile Memory Cells Based on MoS_2/Graphene Heterostructures. *ACS Nano* **2013**, *7*, 3246–3252.
33. Huang, X.; Zeng, Z.; Zhang, H. Metal Dichalcogenide Nanosheets: Preparation, Properties and Applications. *Chem. Soc. Rev.* **2013**, *42*, 1934–1946.
34. Wu, J.; Li, H.; Yin, Z.; Li, H.; Liu, J.; Cao, X.; Zhang, Q.; Zhang, H. Layer Thinning and Etching of Mechanically Exfoliated MoS_2 Nanosheets by Thermal Annealing in Air. *Small* **2013**, *9*, 3314–3319.
35. Li, H.; Lu, G.; Yin, Z.; He, Q.; Li, H.; Zhang, Q.; Zhang, H. Optical Identification of Single- and Few-Layer MoS_2 Sheets. *Small* **2012**, *8*, 682–686.
36. Sik Hwang, W.; Remskar, M.; Yan, R.; Kosel, T.; Kyung Park, J.; Jin Cho, B.; Haensch, W.; Seabaugh, A.; Jena, D. Comparative Study of Chemically Synthesized and Exfoliated Multilayer MoS_2 Field-Effect Transistors. *Appl. Phys. Lett.* **2013**, *102*, 043116.
37. Wilson, J. A.; Yoffe, A. D. Transition Metal Dichalcogenides Discussion and Interpretation of Observed Optical, Electrical and Structural Properties. *Adv. Phys.* **1969**, *18*, 193–335.
38. Neudeck, G. W.; Pierret, R. F. *The PN Junction Diode (Modular Series on Solid States Devices)*; Addison-Wesley Publishing: Reading, MA, 1989; Vol. 2.
39. Chan, J.; Balakchiev, M.; Thron, A.; Chapman, R.; Riley, D.; Song, S.; Jain, A.; Blatchford, J.; Shaw, J.; van Benthem, K. PtSi Dominated Schottky Barrier Heights of Ni (Pt) Si Contacts Due to Pt Segregation. *Appl. Phys. Lett.* **2013**, *102*, 123507.
40. Schroder, D. K. *Semiconductor Material and Device Characterization*, 3rd ed.; John Wiley & Sons: New York, 2006.
41. Wagner, C. D. *Handbook of X-ray Photoelectron Spectroscopy: A Reference Book of Standard Data for Use in X-ray Photoelectron Spectroscopy*; Perkin-Elmer Corp.: Eden Prairie, MN, 1979.
42. Zhou, W.; Zou, X. L.; Najmaei, S.; Liu, Z.; Shi, Y. M.; Kong, J.; Lou, J.; Ajayan, P. M.; Yakobson, B. I.; Idrobo, J. C. Intrinsic Structural Defects in Monolayer Molybdenum Disulfide. *Nano Lett.* **2013**, *13*, 2615–2622.
43. Inoue, A.; Komori, T.; Shudo, K.-I. Atomic-Scale Structures and Electronic States of Defects on Ar^+-Ion Irradiated MoS_2. *J. Electron Spectrosc.* **2013**, *189*, 11–18.
44. Spalvins, T. A Review of Recent Advances in Solid Film Lubrication. *J. Vac. Sci. Technol., A* **1987**, *5*, 212–219.
45. Gong, C.; Lee, G.; Shan, B.; Vogel, E. M.; Wallace, R. M.; Cho, K. First-Principles Study of Metal−Graphene Interfaces. *J. Appl. Phys.* **2010**, *108*, 123711.
46. Giovannetti, G.; Khomyakov, P. A.; Brocks, G.; Karpan, V. M.; van den Brink, J.; Kelly, P. J. Doping Graphene with Metal Contacts. *Phys. Rev. Lett.* **2008**, *101*, 026803.
47. Bagus, P. S.; Staemmler, V.; Woll, C. Exchangelike Effects for Closed-Shell Adsorbates: Interface Dipole and Work Function. *Phys. Rev. Lett.* **2002**, *89*, 096104.
48. Ranade, P.; Choi, Y.-K.; Ha, D.; Agarwal, A.; Ameen, M.; King, T.-J. In *Tunable Work Function Molybdenum Gate Technology for FDSOI-CMOS*; 2002 Electron Devices Meeting, **2002**; pp 363−366.
49. Ward's Science, https://wardsci.com/.
50. Herrera-Gomez, A.; Hegedus, A.; Meissner, P. L. Chemical Depth Profile of Ultrathin Nitrided SiO_2 Films. *Appl. Phys. Lett.* **2002**, *81*, 1014–1016.

51. Wallace, R. M. *In-Situ* Studies of Interfacial Bonding of High-Kappa Dielectrics for CMOS Beyond 22 nm. In *Physics and Technology of High-K Gate Dielectrics 6*; Kar, S., Landheer, D., Houssa, M., Misra, D., VanElshocht, S., Iwai, H., Eds.; The Electrochemical Society: Pennington, NJ, 2008; Vol. 16, pp 255−271.

ARTICLE